Coplanar Asymmetrical Reduced Graphene Oxide–Titanium Electrodes for Polymer Photodetectors

Shuping Pang, Shubin Yang, Xinliang Feng, and Klaus Müllen**

Photodetectors, which convert light signals into a voltage or current, have been widely used in imaging, spectroscopy, fiber-optic communications, and time-gated distance measurements.[1–3] Recently, polymer photodetectors have become increasingly attractive for detection technologies, owing to their high optical absorption coefficient, flexibility, processability, and potential for low-cost fabrication.[1,3–6]

In general, there are two different types of polymer photodetectors, namely photoconductors and photodiodes, as presented in **Figures 1**a and b.[3,7] Typically, polymer photoconductors (Figure 1a) employ two identical coplanar electrodes sandwiching a semiconducting polymer layer.[3,8,9] Under illumination, the conductance of the semiconductor layer will increase as a result of the formation of photogenerated carriers.[3] The difference of the conductance of the polymer in the light and in the dark is thus proportional to the light intensity. However, large numbers of photogenerated electron–hole pairs can quickly recombine in the channel before they reach the electrodes. In this regard, a narrow channel length (several hundred nanometers) and a high operation voltage are required to efficiently dissociate electron–hole pairs and subsequently sweep them to the electrodes before their recombination.[10] The traditional fabrication methods for narrow electrode gaps strongly depend on the equipment, such as electron-beam (e-beam) lithography and atomic force microscopy (AFM) nanolithography.[11–13] By applying standard e-beam lithographic techniques, the gaps can be as narrow as a few tens of nanometers in width. The second type of polymer photodetector is the photodiode, which is normally fabricated in a sandwich structure, as illustrated in Figure 1b, with two different electrodes, at least one of which is transparent.[3,14–16] In this structure, the distance between the two electrodes can be easily reduced to tens to hundreds of nanometers by controlling the thickness of the semiconducting layer. Most importantly, the electron–hole recombination time can be efficiently delayed in the sandwich structure because of the formation of a built-in potential between the two electrodes. However, the disadvantages of this device are the complicated processing and the light reflection and absorption at the transparent electrode.[3,16–18]

Dr. S. P. Pang, Dr. S. B. Yang, Prof. X. L. Feng, Prof. K. Müllen
Max Planck Institute for Polymer Research
Ackermannweg 10, 55128 Mainz, Germany
E-mail: feng@mpip-mainz.mpg.de;
muellen@mpip-mainz.mpg.de
Prof. X. L. Feng
School of Chemistry and Chemical Engineering
Shanghai Jiao Tong University
800 Dongchuan Road, Shanghai 200240, P. R. of China

DOI: 10.1002/adma.201104211

In this Communication, we present a novel and simple strategy for fabricating coplanar asymmetrical reduced graphene oxide (RGO)–titanium (Ti) electrodes (AGTEs) that can avoid the drawbacks of each type of photodetector and fulfill the requirements of low light consumption and high photosensitivity (Figure 1c). RGO was selected as the hole transport electrode because of its suitable work function (4.75 eV)[19] and high carrier injection efficiency for organic materials such as poly(3-hexylthiophene) (P3HT) and pentacene, which have been demonstrated in organic solar cells and field effect transistors (OFETs). The use of a RGO electrode can reduce the contact resistance between electrode and organic semiconductors.[19–25] We used titanium as the electron transport electrode because of its good chemical stability and suitable work function. The combination of oxygen plasma etching and evaporation allows the patterning of AGTEs with narrow channel length. As a result, the photosensitivity of polymer photodetectors with P3HT or a blend of P3HT with phenyl-C_{61}-butyric acid methyl ester (PCBM) was improved by using AGTEs compared with those constructed on symmetrical electrodes.

The fabrication of coplanar AGTEs is illustrated in **Scheme 1**. First, a graphene oxide (GO) dispersion was spin-coated on a SiO_2/Si substrate and then thermally annealed to render the GO film electrically conductive (Scheme 1a). To define the RGO patterns, aluminum patterns were thermally evaporated through a homemade mask with 1 mm × 2 mm rectangular holes (Figure S1a, Supporting Information) on the 20 nm thick RGO film (Scheme 1b). Subsequently, the silicon/RGO/aluminum substrate was exposed to oxygen plasma to remove the RGO regions not covered by the aluminum. Long-time plasma etching produced an undercut along the edges of the aluminum patterns (Scheme 1c). After 3 min of oxygen etching, a 40 nm thick titanium layer was evaporated through another homemade mask with a 1 mm × 7 mm rectangular hole (Figure S1b, Supporting Information) on top of the aluminum pattern (Scheme 1d). Finally, the RGO and Ti patterns arranged alternately on the silicon substrate were obtained by removing the pre-deposited sacrificial aluminum patterns.

The patterned coplanar AGTEs were characterized by means of optical microscopy (OM) and AFM, as shown in **Figure 2**. It can be seen that the RGO electrodes (white, ca. 1 mm × 2 mm rectangles) and titanium electrodes (darker, ca. 1 mm × 1 mm squares) are alternately deposited on the SiO_2/Si substrate (Figure 2a). The sharp and regular contact edges are noticeable in the AFM image (Figure 2b). Therefore, the areas exposed to the oxygen plasma were completely etched away, while the areas protected by aluminum survived the processing. It was found that a channel length of ca. 500 nm between RGO and titanium electrodes was generated after 3 min of plasma etching. The corresponding height profile (Figure 2c) along the

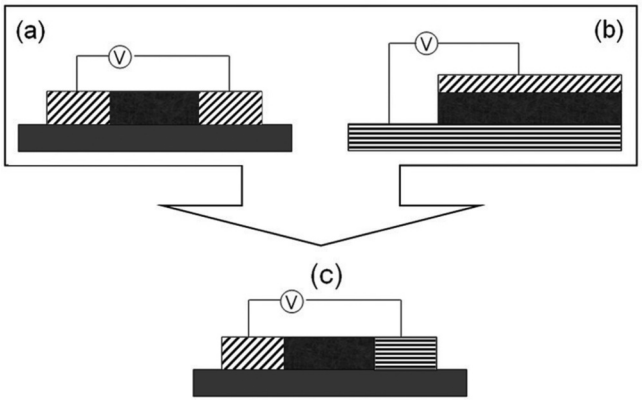

Figure 1. Structural models of a coplanar photoconductor with two symmetrical electrodes (a), a sandwich photodiode with two asymmetrical electrodes (b; one is transparent), and a coplanar photodetector with two asymmetrical electrodes (c).

line in Figure 2b indicates the complete etching of the RGO contacts down to the underlying silicon substrate. The formation of the gap is due to the undercut of the RGO film under

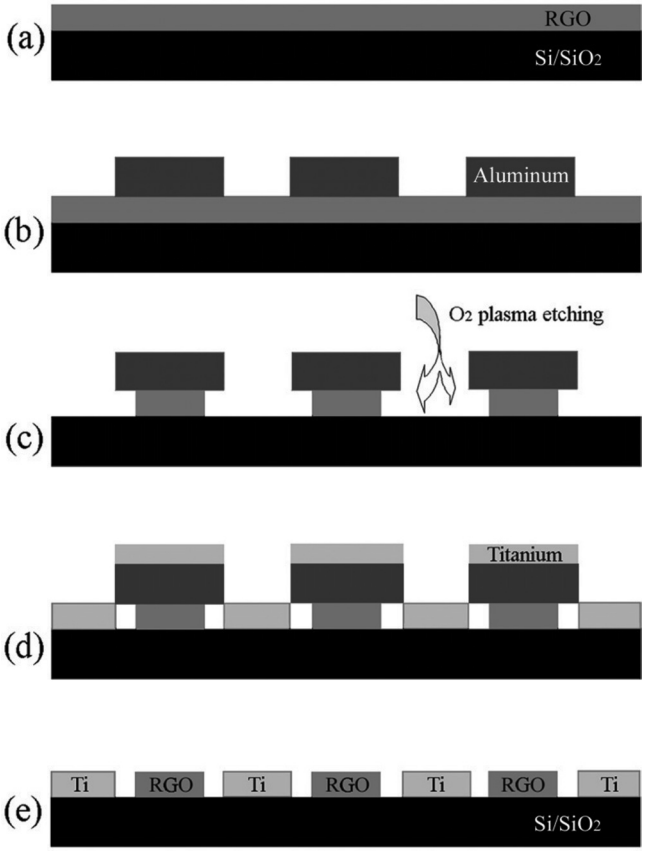

Scheme 1. Schematic illustration of the fabrication process of AGTEs. a) A graphene film was produced by thermal reduction of a GO film. b) Patterned aluminum was evaporated to serve as a sacrificial mask. c) An undercut along the edges of the aluminum patterns was formed by long-time oxygen plasma etching of the graphene film. d) Titanium electrodes were evaporated directly on the etched film. e) Patterned AGTEs were obtained by washing away the sacrificial aluminum layer.

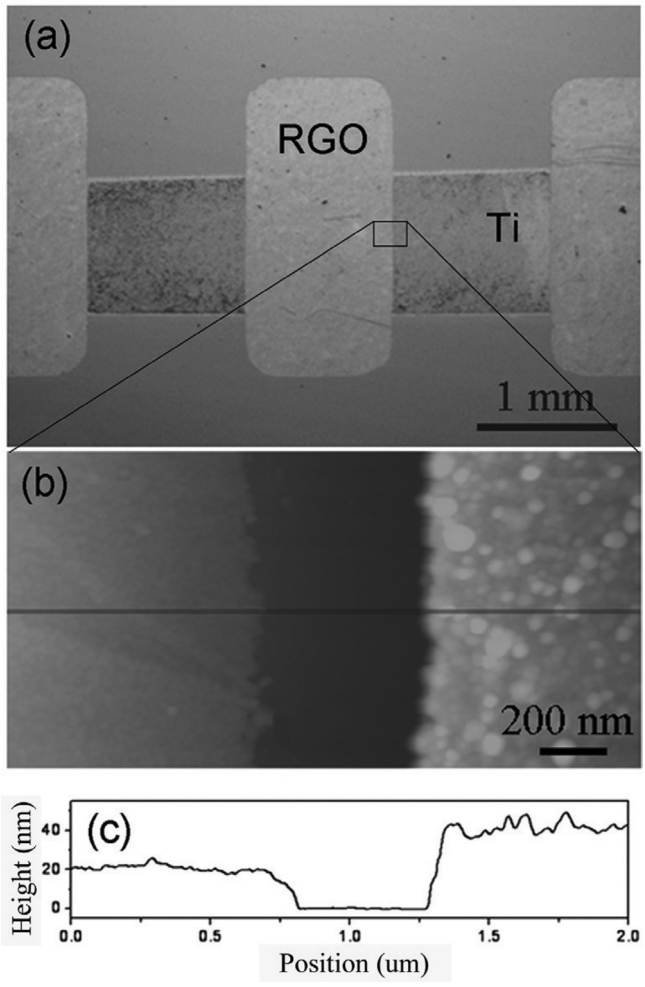

Figure 2. a) OM image of AGTEs; white rectangles are RGO and darker squares are Ti. b) AFM image of the edge of the RGO-Ti electrodes, indicating a channel length of ca. 500 nm. c) Height profile along the line in (b), showing a narrow channel etched down to the underlying SiO_2/Si substrate.

the aluminum patterns. The length of the undercut increases when the oxygen plasma etching time is extended. When we used 20 sccm oxygen flow and 300 W radio frequency (rf) power, the oxygen plasma etching rate of the covered RGO film was ca. 14 nm s^{-1} (Figure S2, Supporting Information). The channel length can therefore be easily adjusted by controlling the oxygen plasma etching time. Additionally, this fabrication process will also allow the fabrication of different asymmetrical electrodes with various work functions, such as graphene/gold and graphene/silver. In view of the application as electrodes in polymer photodetectors, the electron-collecting electrode should possess a work function lower than the energy level of the lowest unoccupied molecular orbital (LUMO) of the photoactive semiconductor. Titanium, with a work function of –4.3 eV, was chosen as a suitable material to collect electrons and block holes from the P3HT layer.[26]

To examine the feasibility of using the as-fabricated coplanar AGTEs in polymer photodetectors, P3HT and a blend of P3HT with PCBM were used as photosensitive materials. Before

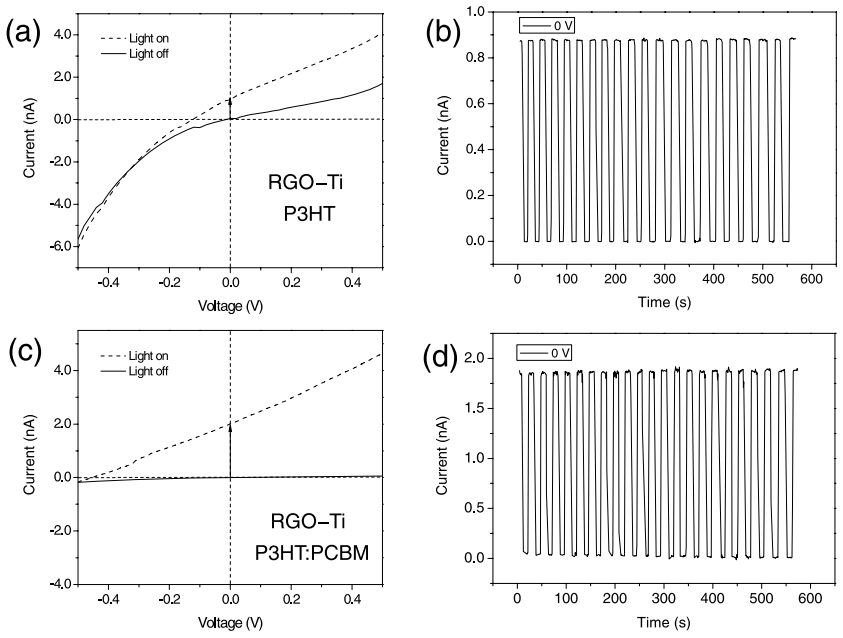

Figure 3. a) *I–V* characteristics of the AGTE-based photodetector with P3HT as the photosensitive material. b) The on/off characteristics of the P3HT photodetector at 0 V bias. c) *I–V* characteristics of the AGTE-based photodetector with the blend P3HT:PCBM as the photosensitive material. d) The on/off characteristics of the P3HT:PCBM photodetector at 0 V bias.

the device fabrication, the substrate with the AGTEs was first treated with 1,1,1,3,3,3-hexamethyldisilazane (HMDS) to render the surface hydrophobic. Subsequently, P3HT or P3HT:PCBM (1:0.8) was spin-coated on top of the modified AGTEs and then annealed at 120 °C for 10 min. The photodetectors were finally tested in a glove box under a light source with intensity of ca. 20 mW cm^{-2}.

Typical current–voltage (*I–V*) characteristics of P3HT photodetectors based on AGTEs are shown in **Figure 3**a. The *I–V* curve in the dark displays an obvious diode behavior. Under illumination, the *I–V* curve moves far away from the origin (0,0). Like a microphotovoltaic cell, the AGTE-based photodetector shows an open-circuit voltage (V_{oc}) of 0.12 V and a short-circuit current (I_{sc}) of 0.98 nA (Figure 3a). The large difference of the currents in the dark and under illumination around the origin (0,0) allows the device to be run at very low bias voltage, offering the possibility of working at low energy consumption. Figure 3b reveals the on/off characteristics of the photodetector at 0 V bias. The current of the devices is rather low in the dark, whereas it jumps sharply by more than three orders of magnitude upon irradiation (ca. 20 mW cm^{-2}), indicating high photosensitivity. Further, switching the shielded light alternately on and off causes the current of the devices to exhibit two distinct steady states: the "low" current state in the dark and the "high" current state in the light, as shown in Figure 3b. Additionally, the on-current of the photodetector measured with a light intensity of 10 mW cm^{-2} at 0 V had a value of 0.48 nA, which is almost half of that when working under 20 mW cm^{-2}, indicating a linear trend with the light intensity.

In order to further improve the photosensitivity of the P3HT photodetector, PCBM can be introduced as an electron-acceptor material, which can promote the dissociation efficiency of the excitons or hole–electron pairs into free holes and electrons at the surfaces of the P3HT:PCBM layer.[27–30] The performance of the P3HT:PCBM photodetector based on the as-fabricated AGTEs is presented in Figures 3c,d. The *I–V* characteristic under illumination (Figure 3c) also displays a typical photodiode character with V_{oc} = 0.46 V and I_{sc} = 2.0 nA. Both V_{oc} and I_{sc} are obviously higher than those of the P3HT photodetectors described above, owing to a more efficient dissociation of the excitons into free electrons, resulting in high photosensitivity when the light is switched on and off (Figure 3d).

To gain an in-depth understanding of the influence of asymmetrical electrodes on the performance of photodetectors, two reference devices based on symmetrical gold contacts with a channel length of 5 μm were investigated. As indicated in **Figures 4**a,c, the diode properties could not be observed when either P3HT or P3HT/PCBM

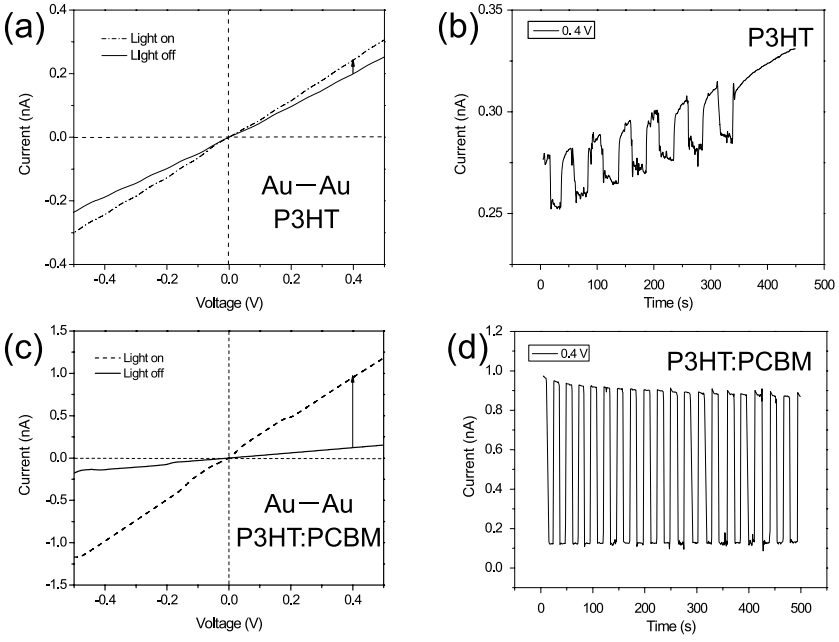

Figure 4. a) *I–V* characteristics of the symmetrical gold electrode–based photodetector with P3HT as the photosensitive material. b) The on/off characteristics of the P3HT photodetector at 0.4 V. c) *I–V* characteristics of the symmetrical gold electrode–based photodetector with the P3HT:PCBM blend as photosensitive material. d) The on/off characteristics of the P3HT:PCBM photodetector at 0.4 V.

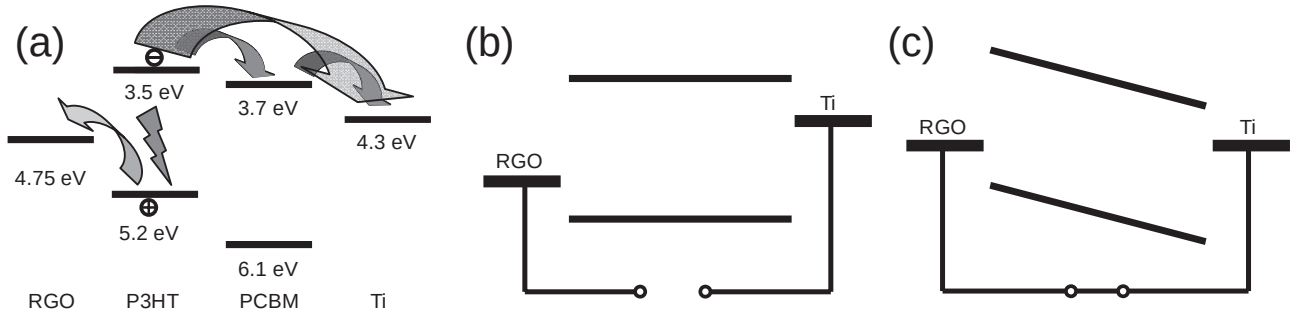

Figure 5. a) A schematic representation of charge transfer and transport as an energy level diagram. b,c) Simplified principles of device function for organic semiconducting layers between two metallic electrodes: open-circuit (flat-band) condition (b) and short-circuit condition (c).

was utilized as the photosensitive material. In this way, a high applied bias voltage was required in order to achieve efficient exciton dissociation. However, the applied bias voltage can also exert an influence on the background current. For instance, the *I–V* curves of a P3HT photodetector measured at 0.4 V bias shows a small variation between the conditions in the dark and under light (Figure 4a). The photocurrent and the dark current are of the same order and the on/off ratio is calculated to be less than 2. Additionally, the current of the photodetector increases and decreases more slowly than that of the P3HT photodetector based on the AGTEs when the light is turned on and off (Figures 3b,d). This can be attributed to the inefficient dissociation of holes and electrons in P3HT under illumination.[10,27] After introduction of the electron acceptor PCBM, both the on/off ratio and the photoresponse time were improved, as demonstrated in Figure 4d. The on/off ratio of the P3HT:PCBM photodetector at 0.4 V is ca. 10, about five times that of the pure P3HT photodetector (Figure 4b). However, the on/off characteristic is not reversible, with a decreasing on-current with repeated on/off operation (Figure 4d).

As can be seen, the P3HT and PCBM photodetectors based on the as-fabricated coplanar AGTEs display improved performance compared with that based on the symmetrical gold electrodes (Table S1, Supporting Information).[10,27] The improvement is attributed to a "built-in" potential, which is governed by the difference of the work functions between the two electrodes.[17,22,31,32] The energy band diagrams of the photoactive materials and the asymmetrical electrodes are illustrated in **Figure 5**a, while the corresponding simplified energy band diagrams are shown in Figure 5b. When the external circuit is shorted, the energy levels of the graphene and titanium electrodes are rectified to the same value and an internal "built-in" electrical field can be produced in the photoactive layer (Figure 5c). In this case, the photoinduced holes and electrons in the polymer layer can quickly move to the opposite electrodes, resulting in the improved photosensitivity. Additionally, the presence of a built-in potential is also beneficial for low-voltage operation, fulfilling the requirement of low energy consumption for future photodetectors.

In summary, we have demonstrated the fabrication of coplanar asymmetrical graphene-titanium electrodes. The fabrication technology involving evaporation of a protective layer and oxygen plasma etching is simple and suitable for patterning electrodes with narrow gaps of several hundred nanometers. The P3HT photodetectors based on the patterned graphene-titanium electrodes result in improved photosensitivity because of the narrow gap and the "built-in" potential originating from the different electrodes, which can efficiently dissociate the excitons into free holes and electrons and then quickly drive them to the opposite electrodes. The easy processing, high photosensitivity, high on/off ratio, and low energy consumption make coplanar asymmetrical electrodes promising in the field of photoelectric devices.

Experimental Section

Preparation of the asymmetrical RGO-Ti electrodes: First, a GO dispersion prepared from natural graphite by the Hummers method was sonicated for 3 h and then spin-coated on a SiO_2/Si substrate. Then the GO film was thermally reduced at 1000 °C for 30 min with a heating rate of 1 °C min^{-1}. The conductivity of the RGO film is ca. 500 S cm^{-1}, which was measured by a standard four-point probe system with a Keithley 2700 Multimeter (probe spacing: 0.635 mm, $R_s = 4.5324\ V/I$). Subsequently, a 60-nm thick aluminum layer was thermally evaporated under vacuum on the RGO film through a homemade mask with 1 mm × 2 mm rectangular holes. The substrate was then exposed in an oxygen plasma cleaner (Plasma System 200) for 3 min with 20 sccm oxygen flow and 300 W rf power. Then a 40 nm thick titanium layer was evaporated on top of the aluminum pattern through another homemade mask with a 1 mm × 7 mm rectangular hole on top of the aluminum patterns. Finally, the asymmetrical RGO-Ti electrodes were obtained after removing the aluminum by immersing the sample in a 5% HNO_3 solution for 60 min.

Device fabrication and measurements: A chloroform solution of P3HT (5 mg mL^{-1}, 4002-E, Rieke Metals, Inc.) or a mixture of P3HT (5 mg mL^{-1}) and PCBM (4 mg mL^{-1}, Aldrich 684430) was spin-coated at 2000 rpm for 40 s on top of the asymmetrical RGO-Ti electrodes. The photodetectors were tested in a glove box under nitrogen atmosphere with a Keithley SCS 4200 semiconductor characterization system. The light of a Nikon microscope (SMZ1000, ca. 20 mW cm^{-2}) was directly used to switch on the photodiode.

Supporting Information

Supporting Information is available from the Wiley Online Library or from the author.

Acknowledgements

This work was financially supported by the Max Plank Society through the program ENERCHEM, National Basic Research Program of China

(2012CB933400), DFG Priority Program SPP 1355, DFG MU 334/32-1, DFG Priority Program SPP 1459, and ESF Project GOSPEL (Ref Nr: 09-EuroGRAPHENE-FP-001), EU Project GENIUS and ERC grant on NANOGRAPH.

Received: November 2, 2011
Revised: January 5, 2012
Published online: February 20, 2012

[1] X. Gong, M. H. Tong, Y. J. Xia, W. Z. Cai, J. S. Moon, Y. Cao, G. Yu, C. L. Shieh, B. Nilsson, A. J. Heeger, *Science* **2009**, *325*, 1665.
[2] G. Konstantatos, I. Howard, A. Fischer, S. Hoogland, J. Clifford, E. Klem, L. Levina, E. H. Sargent, *Nature* **2006**, *442*, 180.
[3] G. Konstantatos, E. H. Sargent, *Nat. Nanotechnol.* **2010**, *5*, 391.
[4] G. A. O'Brien, A. J. Quinn, D. A. Tanner, G. Redmond, *Adv. Mater.* **2006**, *18*, 2379.
[5] B. Pradhan, K. Setyowati, H. Y. Liu, D. H. Waldeck, J. Chen, *Nano Lett.* **2008**, *8*, 1142.
[6] S. Liu, J. M. Li, Q. Shen, Y. Cao, X. F. Guo, G. M. Zhang, C. Q. Teng, J. Zhang, Z. F. Liu, M. L. Steigerwald, D. S. Xu, C. Nuckolls, *Angew. Chem. Int. Ed.* **2009**, *48*, 4759.
[7] S. Wan, J. Guo, J. Kim, H. Ihee, D. L. Jiang, *Angew. Chem. Int. Ed.* **2009**, *48*, 5439.
[8] V. Sukhovatkin, S. Hinds, L. Brzozowski, E. H. Sargent, *Science* **2009**, *324*, 1542.
[9] H. Y. Chen, M. K. F. Lo, G. W. Yang, H. G. Monbouquette, Y. Yang, *Nat. Nanotechnol.* **2008**, *3*, 543.
[10] Y. Cao, S. Liu, Q. Shen, K. Yan, P. J. Li, J. Xu, D. P. Yu, M. L. Steigerwald, C. Nuckolls, Z. F. Liu, X. F. Guo, *Adv. Funct. Mater.* **2009**, *19*, 2743.
[11] T. Takahashi, T. Takenobu, J. Takeya, Y. Iwasa, *Adv. Funct. Mater.* **2007**, *17*, 1623.
[12] S. Cho, J. Yuen, J. Y. Kim, K. Lee, A. J. Heeger, *Appl. Phys. Lett.* **2007**, *90*, 063511.
[13] J. M. Mativetsky, A. Liscio, E. Treossi, E. Orgiu, A. Zanelli, P. Samori, V. Palermo, *J. Am. Chem. Soc.* **2011**, *133*, 14320.
[14] P. Peumans, V. Bulovic, S. R. Forrest, *Appl. Phys. Lett.* **2000**, *76*, 3855.
[15] T. Rauch, M. Boberl, S. F. Tedde, J. Furst, M. V. Kovalenko, G. N. Hesser, U. Lemmer, W. Heiss, O. Hayden, *Nat. Photonics* **2009**, *3*, 332.
[16] N. C. Greenham, X. G. Peng, A. P. Alivisatos, *Phys. Rev. B* **1996**, *54*, 17628.
[17] Y. H. Chang, C. M. Liu, Y. C. Tseng, C. Chen, C. C. Chen, H. E. Cheng, *Nanotechnology* **2010**, *21*, 225602.
[18] S. W. Clark, J. M. Harbold, F. W. Wise, *J. Phys. Chem. C* **2007**, *111*, 7302.
[19] A. Liscio, G. P. Veronese, E. Treossi, F. Suriano, F. Rossella, V. Bellani, R. Rizzoli, P. Samori, V. Palermo, *J. Mater. Chem.* **2011**, *21*, 2924.
[20] Q. Su, S. P. Pang, V. Alijani, C. Li, X. L. Feng, K. Müllen, *Adv. Mater.* **2009**, *21*, 3191.
[21] S. P. Pang, H. N. Tsao, X. L. Feng, K. Müllen, *Adv. Mater.* **2009**, *21*, 3488.
[22] M. Y. Liu, C. H. Chang, C. H. Chang, K. H. Tsai, J. S. Huang, C. Y. Chou, I. J. Wang, P. S. Wang, C. Y. Lee, C. H. Chao, C. L. Yeh, C. I. Wu, C. F. Lin, *Thin Solid Films* **2010**, *518*, 4964.
[23] U. J. Kim, H. Bin Son, E. H. Lee, J. M. Kim, S. C. Min, W. Park, *Appl. Phys. Lett.* **2010**, *97*, 032117.
[24] S. P. Pang, Y. Hernandez, X. L. Feng, K. Müllen, *Adv. Mater.* **2011**, *23*, 2779.
[25] Z. F. Liu, Q. Liu, Y. Huang, Y. F. Ma, S. G. Yin, X. Y. Zhang, W. Sun, Y. S. Chen, *Adv. Mater.* **2008**, *20*, 3924.
[26] S. Cho, K. Lee, A. J. Heeger, *Adv. Mater.* **2009**, *21*, 1941.
[27] H. F. Zhu, T. Li, Y. J. Zhang, H. L. Dong, J. S. D. Song, H. P. Zhao, Z. M. Wei, W. Xu, W. P. Hu, Z. S. Bo, *Adv. Mater.* **2010**, *22*, 1645.
[28] I. W. Hwang, D. Moses, A. J. Heeger, *J. Phys. Chem. C* **2008**, *112*, 4350.
[29] M. S. Arnold, J. D. Zimmerman, C. K. Renshaw, X. Xu, R. R. Lunt, C. M. Austin, S. R. Forrest, *Nano Lett.* **2009**, *9*, 3354.
[30] G. Yu, J. Wang, J. McElvain, A. J. Heeger, *Adv. Mater.* **1998**, *10*, 1431.
[31] B. Zimmermann, M. Glatthaar, M. Niggemann, M. Riede, A. Hinsch, *Thin Solid Films* **2005**, *493*, 170.
[32] T. Mueller, F. N. A. Xia, P. Avouris, *Nat. Photonics* **2010**, *4*, 297.